Nanoscale

Accepted Manuscript

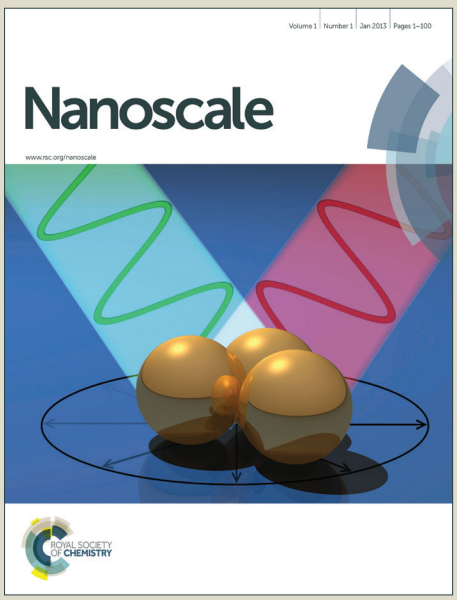

ROYAL SOCIETY OF CHEMISTRY

www.rsc.org/nanoscale

Nanoscale

Dynamic Article Links ►

Cite this: DOI: 10.1039/c0xx00000x

www.rsc.org/xxxxxx

ARTICLE TYPE

Antioxidant Chemistry of Graphene-Based Materials and its Role in Oxidation Protection Technology

Yang Qiu[a], Zhongying Wang[b], Alisa C.E. Owens[a], Indrek Kulaots[a], Yantao Chen[b], Agnes B. Kane[c], Robert H. Hurt*[a]

Received (in XXX, XXX) Xth XXXXXXXXX 20XX, Accepted Xth XXXXXXXXX 20XX
DOI: 10.1039/b000000x

Two-dimensional nanomaterials have potential as a new class of antioxidants that combine physical barrier function with ultrahigh surface area for free radical scavenging. This work presents the first measurements of the chemical reactivities of graphene-based materials toward a set of model free radicals and reactive oxygen species using electron paramagnetic resonance spectroscopy (EPR) and sacrificial dye protection assays. Graphene-based materials are shown to protect a variety of molecular targets from oxidation by these species, and to be highly effective as hydroxyl-radical scavengers. When hydroxyl radical is produced photolytically, the overall antioxidant effect is a combination of preventative antioxidant activity (UV absorption) and ·OH radical scavenging. Few-layer graphene is more active than monolayer graphene oxide, despite its lower surface area, which indicates that the primary scavenging sites are associated with the sp^2-carbon network rather than oxygen-containing functional groups. To explain this trend, we propose that GO is a weak hydrogen donor, due to the non-phenolic nature of most OH groups on GO, which reside at basal sp^3-carbon sites that do not allow for radical resonance stabilization following hydrogen donation. As an example application of graphene antioxidant behavior, we show that encapsulation of TiO_2 nanoparticles in graphene nanosacks reduces undesired photo-oxidative damage to nearby organic target molecules, which suggests graphene encapsulation as a new approach to managing adverse environmental or health impacts of redox-active nanomaterials.

Keywords:

antioxidant; free radical; metal ion toxicity; superoxide; titanium oxide; graphene.

1. Introduction

Reactive oxygen species (ROS) play an important role in food spoilage,[1] oil rancidification,[1] polymer degradation,[2] and damage to biological structures that include cell membranes, protein structures, and DNA.[3-5] Oxidation protection is a broad area of chemical and biochemical technology with applications in nutrition,[6] food and pharmaceutical formulations,[4, 7, 8] biomedical implants,[9] topical protection,[10] cosmetics,[7] metal corrosion,[11] wound healing therapies,[12] and the long-term stabilization of chemical products and polymer materials.[2] Graphene-based materials have been explored as two-dimensional physical barriers that restrict access of oxidants to surfaces, but the potential for graphene-based materials as *chemical agents* in oxidation protection has not been systematically explored to our knowledge.

Low temperature oxidation protection often involves destroying or inhibiting the formation of ROS, which form by the uncontrolled and undesired partial reduction of molecular oxygen in the presence of Fenton-active metal catalysts, material surfaces, or UV radiation. Carbon nanomaterials can generate ROS through surface reactions, often involving defect or heteroatom sites,[13, 14] or through transition metal impurities.[15-17] A variety of heteroatoms can be present in chemically modified nanocarbons and these may govern ROS generation or toxicity.[18-20] Carbon nanomaterials may also scavenge ROS, as reported by several studies focused on fullerenes, carbon nanotubes (CNTs) and functionalized carbon dots.[21-27] Oxidation protection by carbon materials may involve radical adduct formation at sp^2 carbon sites, which delocalizes spin across the conjugated graphenic backbone[28] and leads to destruction of the radical following second adduct formation;[25, 27] through electron transfer;[29, 30] through hydrogen donation from functional groups;[31] or through chelation of transitional metal ions and inhibition of Fenton-based radical generation.[32-34] Graphene-based materials may

show one or more of these important behaviors, but this has not been confirmed, and the relative activity of different members of the graphene family, or toward different radicals or ROS is unknown.

Here we investigate the basic chemical activity of graphene oxide (GO), reduced graphene oxide (rGO), and few-layer graphene (FLG) against various ROS: hydroxyl radical, superoxide, peroxides/peroxyls, and the model stable radicals 2,2-diphenyl-1-picrylhydrazyl (DPPH) and 2,2'-azino-bis(3-ethylbenzothiazoline -6-sulphonic acid) (ABTS) radical cation. Hydroxyl radicals (˙OH) are generated *in situ* through Fenton chemistry or UV irradiation, and detected by electron paramagnetic resonance (EPR). Additional experiments are designed to test whether suspended graphene sheets can protect organic dyes from destruction by *in situ* generated ˙OH. Multiple experiments here show that GO is an effective scavenger of ˙OH and can protect water soluble dyes and spin traps from oxidation. FLG is more active despite its lower surface area, suggesting that the main scavenging sites are on the pristine graphenic basal plane and are not associated with H-donation from hydroxyl groups. In experiments involving UV-induced ˙OH generation, some of the protective effect is attributed to UV absorption by graphene in addition to radical scavenging. These behaviors are discussed in relations to the physical and chemical structures of GO and FLG. Finally, we demonstrate one application, in which graphene nanosack encapsulation is used to reduce ROS generation and oxidative damage that are undesired side effects when TiO_2 nanoparticles are used for UV protection.

2. Results

2.1. Characterization

Figure 1 summarizes the properties of the graphene-based materials synthesized and used in this study. The GO has typical lateral dimensions from 1–5 µm (Figure 1B) and is primarily in monolayer form (Figure 1C), which exhibits ~2600 $m^2 g^{-1}$ surface area when fully dispersed in aqueous media. In contrast, the FLG and rGO materials are multilayer structures that were obtained/fabricated as dry powders that must be dispersed in the aqueous test media. Vapor adsorption methods provide information on surface area and pore structure of these graphene-based powders (Figure 1D), which are lower (663-713 $m^2 g^{-1}$) than the monolayer surface area due to face-to-face association of individual layers (or incomplete exfoliation in some cases). The surface area of rGO powders measured by N_2 probe is only 10 $m^2 g^{-1}$ (data not shown) but 680 $m^2 g^{-1}$ when measured by CO_2 probe. This is a well-known effect in carbon materials ($Area_{nitrogen} << Area_{carbon-dioxide}$) that indicates the presence of super-micropores near the molecular diameter of N_2 (0.3-0.84 nm) that are not accessible to the N_2 probe at the low temperature of the experiment (77 K) due to diffusional limitations but are accessible to CO_2 (a similarly sized molecule) at the higher temperatures used to obtain those isotherms (273 K).[35] The presence of these ultrafine micropores capable of molecular sieving has been observed previously in rGO films.[36] Raman characterization (Figure 1A) shows lower defect densities on FLG, as expected for this material that has not been subjected to permanganate-mediated basal surface oxidation.

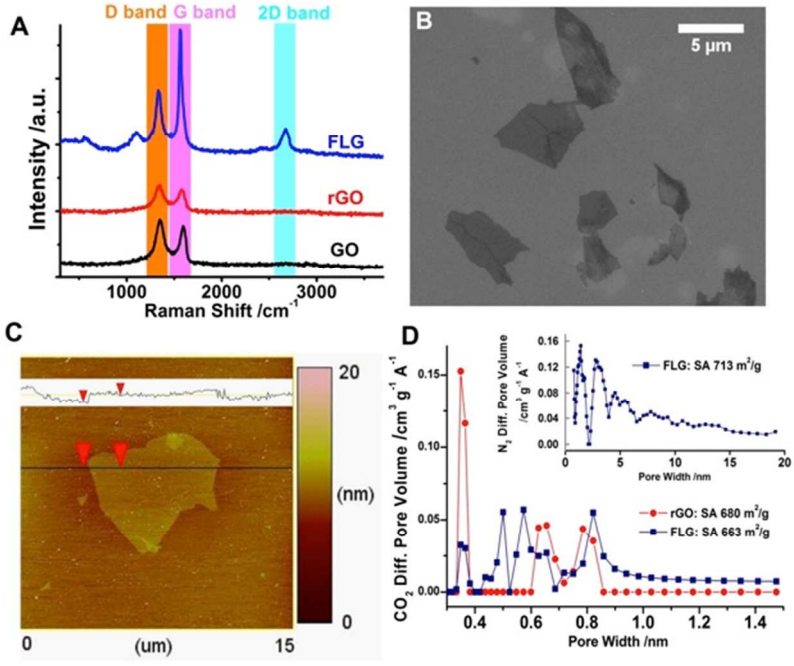

Figure 1. Graphene material characterization. A: Raman spectra; B: Typical SEM image showing 1-5 µm nominal lateral dimension for GO sheets on silicon substrate; C: AFM image of typical GO sheet. Line scan shows 1.04 nm step height indicating monolayer GO; D: Differential pore size distributions (Diff. PSD) for rGO and FLG as bulk dry powders as probed by CO_2 at 273 K (main plot) and N_2 at 77 K (inset). The total surface areas near 700 $m^2 g^{-1}$ indicate that the materials are composed of multilayer stacks of approximately 3-4 layers (2600/700). The N_2 Diff. PSD show characteristic modes with a periodic spacing of 1-2 nm, which has been interpreted as the pores formed by irregular stacking of 1-2 nm plate-like structures [37]

2.2. Hydroxyl radical scavenging

Multiple assays were employed to characterize the ability of graphene-based materials to scavenge ·OH, which is a highly reactive radical implicated in a wide range of undesired low-temperature oxidation processes and biochemical reactions. Figure 2 shows the ability of (monolayer) GO in suspension to protect organic molecules in solution from ·OH oxidation. Here the ·OH is generated by Fenton chemistry ($Fe^{2+} + H_2O_2 \rightarrow \cdot OH + OH^- + Fe^{3+}$), and the oxidizable target molecules are tracked by UV-vis. spectroscopy (for the case of phenol red, Figure 2A) or by EPR (for DMPO, which forms the DMPO-OH radical adduct with its characteristic EPR spectrum shown in Figure 2B). The protective effect of GO in both cases is dose-dependent and quite pronounced above 100 μg mL^{-1} (100 ppm).

We considered the possibility that the observed effect was due to inhibition of the Fenton reaction by iron complexation at oxygen-containing functional groups on GO rather than radical scavenging, and carried out two control experiments to evaluate this possibility. Figure 2C shows that the GO protective effect is still observed when an excess of ethylenediaminetetraacetic acid (EDTA) is added, whose strong chelation ability prevents iron complexation with GO. (Separate experiments involving iron analysis by inductively coupled plasma-atomic emission spectroscopy (ICP-ES) show that GO does bind iron in these solutions, but not in the presence of the much stronger complexing agent EDTA – see ESI). The EDTA-Fe complex retains some redox activity, which leads to phenol red oxidation and DMPO adduct formation, and these oxidation processes are still inhibited by GO, confirming the presence of the radical scavenging mechanism. Further, Figure 2D shows that GO is still protective when ·OH is generated by sonochemistry, which involves homolytic cleavage of H_2O_2 [38, 39] by a mechanism that does not involve iron. Another possible artifact here would be the direct reaction between GO and H_2O_2 used in the Fenton-generation of ·OH, but this reaction was found to be slow by direct measurement of H_2O_2 (see ESI) and through a later assay (Figure 6A). Overall, it is clear that dispersed monolayer GO at 100 ppm concentration is quite active as an ·OH scavenger.

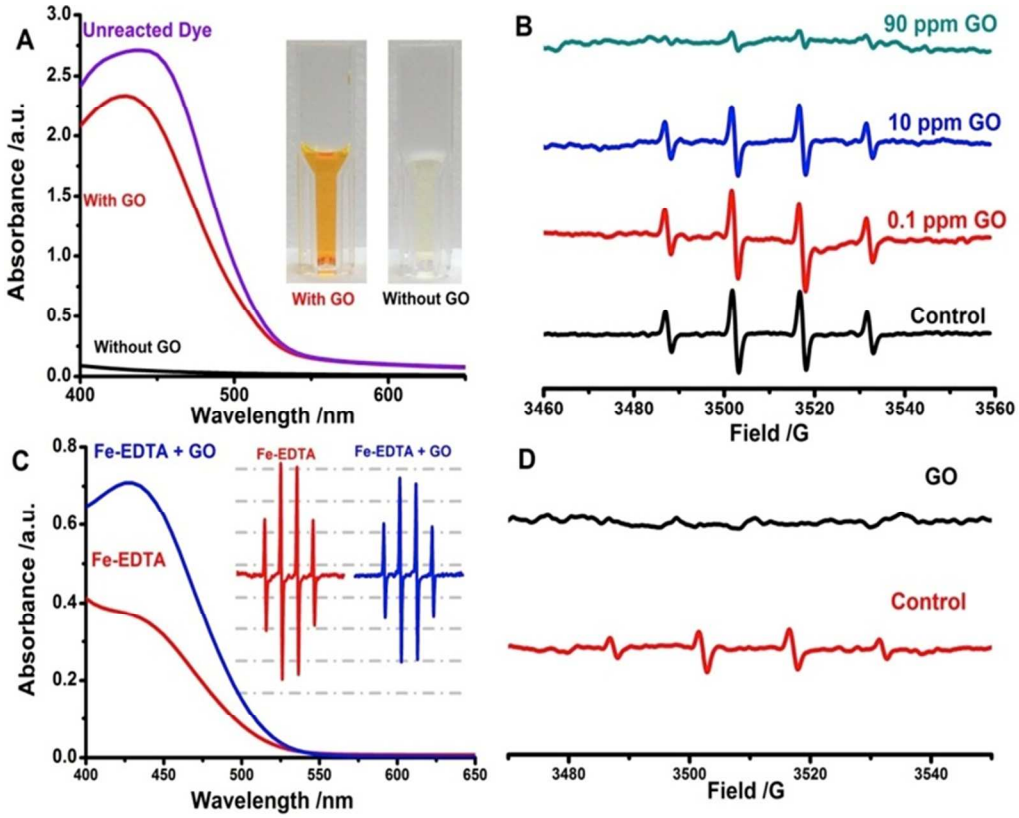

Figure 2. GO as a hydroxyl-radical scavenger. A: Addition of 100 ppm GO protects phenol red from oxidation by Fenton-generated ·OH over 8 hrs. B: Addition of GO protects the spin-trap DMPO from oxidation by Fenton-generated ·OH detected by EPR spectroscopy. The protective effect is concentration dependent over the range 0.1-90 ppm GO. C: Both phenol red monitoring and EPR were used to test if the GO-mediated protective effect is due to radical scavenging or Fenton suppression by Fe-binding. The protective effect of GO is still present when GO-Fe binding is suppressed by EDTA, confirming the importance of radical scavenging. D: GO also protects DMPO when ·OH is generated sonochemically, in a non-Fenton assay, providing additional evidence for true radical scavenging. All experiments were done in PBS (pH 3.5).

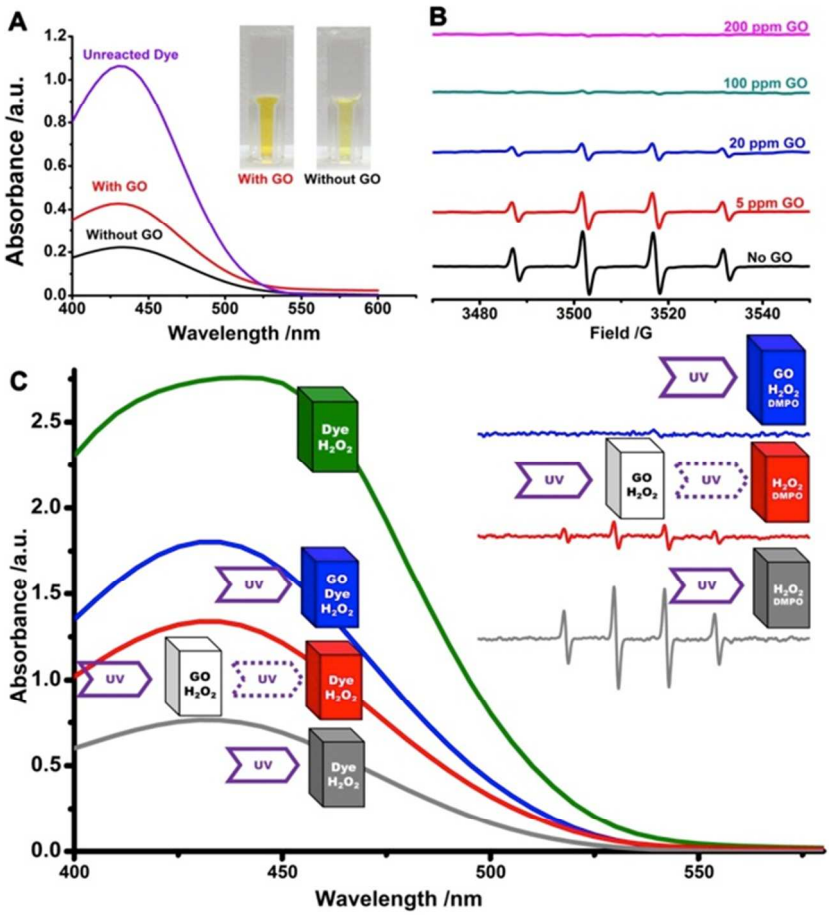

Figure 3. GO antioxidant function in systems with ·OH generation by UV-irradiation of hydrogen peroxide. A: GO (200 ppm) retards phenol red oxidation, B: GO (200 ppm) suppresses DMPO-OH radical adduct formation; C: Mechanism - additional experiments to separate the effects of radical scavenging and UV adsorption by GO. Placing GO in the UV beam path but physically separated from the dye reveals the contribution of UV absorption to the total protective effect of GO. Results from both dye monitoring (main plot, 200 ppm GO) and EPR (inset, 100 ppm GO) show that the protective effect of GO in these systems is a combination of UV absorption and radical scavenging.

Figure 3 characterizes the behavior of GO in systems where ·OH is generated by water photolysis rather than Fenton chemistry. Here again, suspended monolayer GO shows some protective effect for phenol red (Figure 3A) and for DMPO (Figure 3B). These effects cannot be related to iron binding, but may involve ·OH scavenging or UV absorption that inhibits the original ·OH generation. Figure 3C shows the results of special control experiments to determine the separate contributions of UV absorption and ·OH scavenging. The red curves (second from bottom) were generated by placing the GO in a separate cuvette isolated from the target molecule, but in the beam path where UV absorption can occur but not scavenging in a manner that could protect the phenol red (main plot) or the DMPO (inset). These results show that the antioxidant effect of GO here is a combination of UV absorption and ·OH scavenging. The UV absorption is a type of preventative antioxidation mechanism, and because this absorption is the result of integration along the total beam path, it should be more important in thicker systems (tissues, bulk materials or thick films) and less important in thin film systems according to Beer-Lambert law.

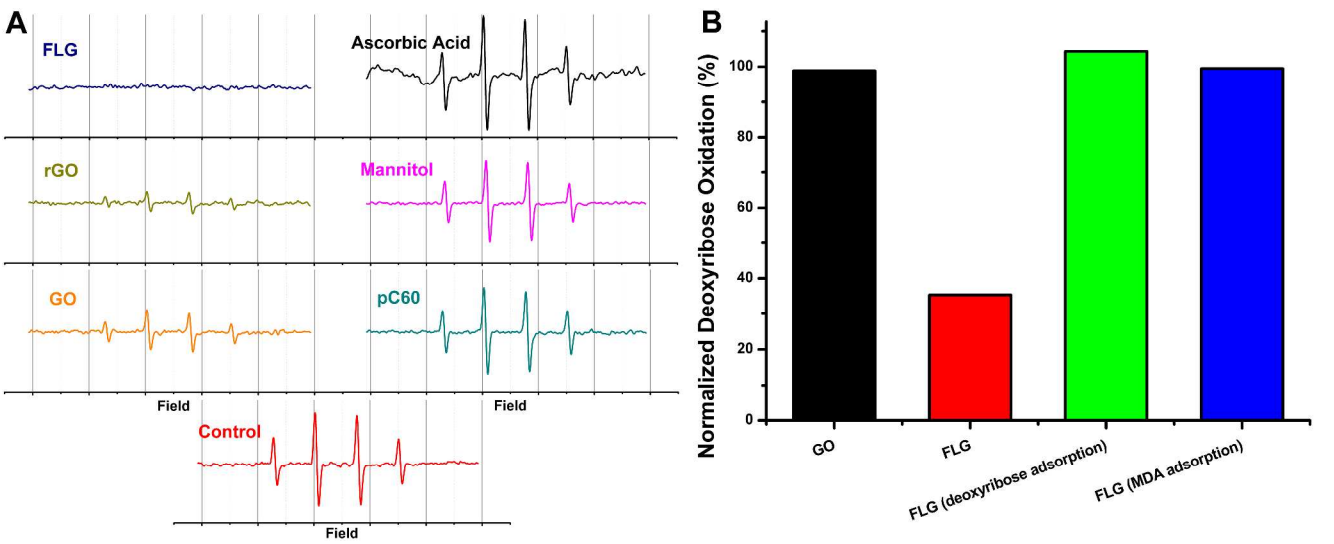

Figure 4. Comparison of different graphene-based materials as ·OH scavengers. A: EPR spectra of DMPO-OH· adduct formed through 20 min Fenton reaction- in the presence of 200 ppm graphene-based and reference materials. Radical scavenging potency follows rank order: FLG > rGO > GO > mannitol> pC60. Ascorbic acid is a pro-oxidant under these conditions. B: MDA assay showing 100 ppm FLG (red bar, second bar from left) is more active than 100 ppm GO (black bar, first bar from left) in protection of 100 mM deoxyribose from Fenton-generated ·OH oxidation. The right-hand two bars show control experiments that rule out adsorptive artifacts in the FLG experiment. When FLG is added and removed before the oxidation step (green bar, third bar from left), there is no effect (which rules out physical adsorption of deoxyribose). When FLG is added and removed after the oxidation (blue bar, fourth bar from left), there is also no effect (which rules our physical adsorption of the deoxyribose oxidation products).

An important goal of this work was to explore the relative antioxidant activity of different members of the graphene material family as a guide to material selection and design.

We attempted to use all three materials (GO, rGO, FLG) in all assays, but found that the hydrophobic varieties (rGO, FLG) produced adsorptive artifacts, especially in those assays involving dye destruction, due to the well-known affinity of pristine carbon surfaces for conjugated dyes.[40] We therefore focused on GO in most assays, but devised special experiments to compare the three materials in a reliable manner free of artifacts. Figure 4A compares the ·OH scavenging activities of GO, rGO, FLG, and reference antioxidants using the DMPO spin trap protection assay with Fenton-generated ·OH and EPR detection of DMPO-OH as above. At 200 ppm, all the graphene-based materials are active scavengers and are more active than the reference antioxidants mannitol and the fullerene derivative pyrrolidine tris-acid C_{60} (pC60), which is a commercially available water-soluble fullerene derivative reported to show antioxidant activity.[23] Ascorbic acid is seen to be a pro-oxidant under these conditions, as has been observed previously,[41] and attributed to its activity in reducing Fe^{3+} to Fe^{2+} for further Fenton reaction with peroxide[10, 42], which accelerates ·OH generation in this assay.

The antioxidant activity of the graphene-based materials toward ·OH falls in the order FLG > rGO > GO. Because monolayer GO has by far the highest surface area, this rank order indicates a much higher area-specific (intrinsic) activity for the pristine or reduced graphene forms (FLG, rGO), an observation that provides insight into the mechanism of antioxidation (see Discussion). The left two bars in Figure 4B shows that FLG is more active than GO in protecting deoxyribose from ·OH attack. We were concerned about artifacts, since the pristine hydrophobic surfaces of the FLG samples can cause significant physical adsorption of dyes and reagents in biological fluids and assays.[40] We therefore carried out an additional assay with deoxyribose as a very soluble hydrophilic target molecule that is not depleted by physical adsorption under these conditions (the right two bars in Figure 4B). Here too FLG is more active indicating that it is an intrinsically better ·OH scavenger than GO. Additional controls indicate that the EPR effects in Figure 4A are not due to FLG interacting with DMPO or its OH adduct (see ESI).

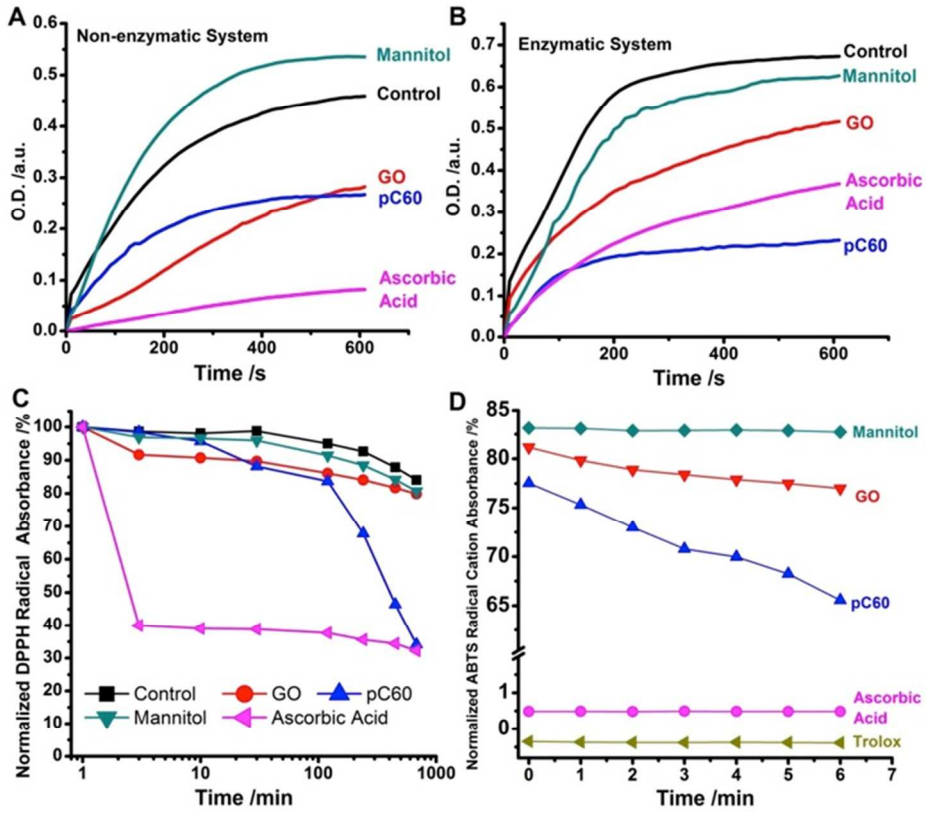

Figure 5. GO interactions with other radical species. A,B: superoxide radical scavenging by GO and reference antioxidants (83 ppm) using nonenzymatic (A) and enzymatic (B) methods of superoxide generation. Superoxide was monitored for 600 s by measuring the absorbance of superoxide-reduced NBT at 560 nm. GO shows modest scavenging activity in this assay. C, D: Interaction of GO and reference antioxidants (100 ppm) with the model stable free radicals DPPH· (C) and $ABTS^{\cdot+}$ radical cation (D). GO shows weak activity relative to the known H-donor antioxidants ascorbic acid and Trolox.

2.3. Other radical and oxidant interactions

Superoxide anion, $O_2^{\cdot-}$, is another important oxygen-centered radical species that forms through the one-electron reduction of molecular oxygen, and is scavenged in biological system by the superoxide dismutase family of antioxidant enzymes that catalyze its destruction through disproportionation to H_2O_2 and O_2.[43] Figure 5 shows the effects of GO on superoxide concentrations following $O_2^{\cdot-}$ generation by non-enzymatic (A) and enzymatic (B) routes. The assay monitors the superoxide-mediated conversion of nitroblue tetrazolium chloride (NBT) to the blue chromagen formazan, which has a characteristic absorption peak at 560 nm.[44] Figure 5A shows that GO shows a modest scavenging effect against superoxide compared to ascorbic acid and pC60, which both have been reported as strong $O_2^{\cdot-}$ scavengers.[23, 45-47] Because the activity is seen in both the enzymatic and non-enzymatic systems, the results cannot be attributed to GO-mediated enzyme deactivation.

In addition to the protection-based, three-molecule (oxidant, target, antioxidant) assays described above, antioxidant activity can also be assessed by measuring the direct reaction rates of candidate antioxidant molecules (here graphene-based materials) with model free radicals of sufficient stability for use in laboratory assays. Figure 5C shows results for the standard radical DPPH·[33, 48, 49] and Figure 5D for $ABTS^{\cdot+}$.[50] GO shows weak activity toward DPPH· in comparison to the known reference antioxidants pC60 and ascorbate.[6] Similarly, GO shows weak but measureable activity toward $ABTS^{\cdot+}$ relative to known antioxidants ascorbate, pC60, and Trolox.[50, 51] Because the quenching of DPPH· and $ABTS^{\cdot+}$ typically occur through hydrogen donation[50, 52] the weak activity of GO here suggests it is a poor H-donor.

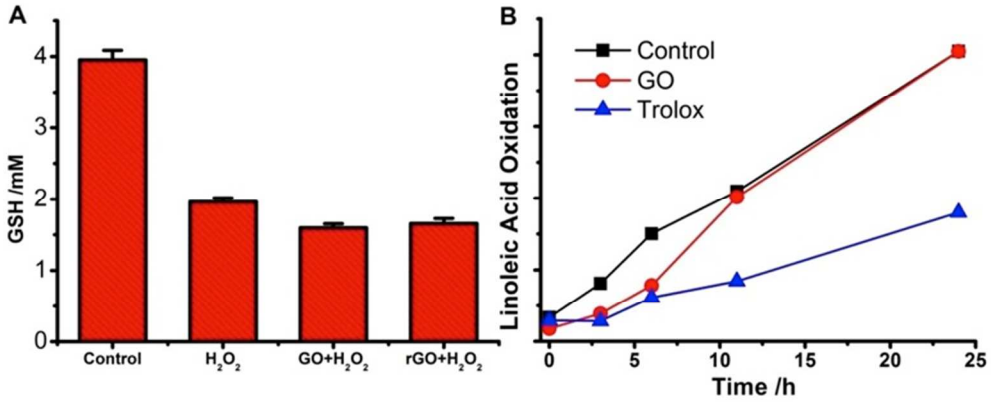

Figure 6. Graphene material activity against hydrogen peroxide (A) and lipid peroxyl radicals (B). A: GO and rGO (100 ppm) shows no protection on 4 mM GSH against oxidation by 1 mM H_2O_2. B: GO (200 ppm) shows weak protection on linoleic acid against oxidation.

Glutathione (GSH) is a key endogenous antioxidant, whose depletion is widely used as a measure of oxidative stress in biological systems.[43, 53, 54] GSH oxidation can be catalyzed by carbon nanotubes[13] and an acellular GSH oxidation assay has been proposed as a measure of pro-oxidant potential for carbon nanomaterials.[13, 14] GSH reacts quickly with hydrogen peroxide [13] and here we carried out experiments to see if GO could inhibit that oxidation and protect GSH. Figure 6A shows that GO has no measurable ability to protect GSH from H_2O_2. Figure 6B shows that the presence of GO caused a slight delay in lipid peroxidation initiated by the azo free-radical initiator 2,2'-azobis(2-amidinopropane) hydrochloride (AAPH) which decomposes by a first order kinetics. Lipid peroxidation is a major cause of food and drug product spoilage and has been implicated in human disease.[3] Here GO shows a weaker antioxidant activity than Trolox, an analog of vitamin E used as a standard reference antioxidant for lipid peroxidation.

3. Discussion

Figures 2-6 provide the first systematic data on the antioxidant behaviors of graphene-based materials. A number of clear patterns are seen: first they are active against ·OH in multiple independent assays, and when present in a well-dispersed state at ~ 100 ppm can protect dissolved organic dyes and spin traps from ·OH oxidation. They show modest activity against superoxide, but are relatively inactive toward hydrogen peroxide, lipid peroxyl radicals, and two stable free radicals ($DPPH^{\cdot}$, $ABTS^{\cdot+}$) that are often used as standard probes to assess the activity of molecular antioxidants. The graphene-based materials show OH radical scavenging activities in the order FLG > rGO > GO, which is in inverse order to their total surface area.

To what extent can this pattern of antioxidant activity be related to the structures of GO or pristine FLG? First we note that graphene materials may also have pro-oxidant activities, and the observed ROS inhibition here is, in principle, the net effect of ROS scavenging and generation, though the high concentrations of externally generated ROS may be expected to overwhelm the material-dependent ROS. We have carried out studies of oxidant production from this set of materials (see ESI), and the order of activity is also FLG > rGO > GO, so pro-oxidant contributions cannot explain the trends seen here for anti-oxidant activity.

The ranking FLG > rGO > GO suggests that the primary actives sites are associated with the pristine graphenic network, rather than oxygen-containing functional groups. We note that the activity of oxygen-containing groups may be pH-dependent, but the high activity of FLG relative to GO is seen at both pH3 and pH7 in separate assays. Most molecular antioxidants that show activity toward $DPPH^{\cdot}$ and $ABTS^{\cdot+}$ are hydrogen donors of the form AH that act through: $AH + R^{\cdot} \rightarrow RH + A^{\cdot}$, where the new radical $A^{\cdot}$ is sufficiently stable not to propagate the free-radical chain reaction. Many H-donor antioxidants for ·OH scavenging act through R-O-H groups where the O-H bond dissociation energy (BDE) is low enough for sufficient reactivity. [31, 55] It is interesting that GO is seen here to be a weak antioxidant in these standard assays, and is thus a poor H-donor antioxidant despite its high hydroxyl content compared with rGO and FLG as shown by the FTIR spectra in ESI (OH/C ratio ~0.25 as reported in literature).[56]

We believe the weak activity of GO as a donor antioxidant is consistent with its chemical structure. Many antioxidants are phenolic compounds,[57] whose radical forms following H-donation are stabilized by resonance structures,[58] in which the unpaired electron can reside on the oxygen atom, or on ortho or para carbons on the adjacent aromatic ring.[59] GO has many hydroxyl groups and also extensive aromaticity in the form of pristine sp^2-carbon domains between oxidized regions, but is not highly active as an H-donor. Most accepted models for GO structure place the OH groups out-of-plane at basal sites, where oxidation of C=C double bonds has created local sp^3 sites that do not offer the adjacent conjugated structure necessary for radical resonant stabilization. Such basal OH groups on GO are not expected to show strong antioxidant activity.

In the absence of basal defects in GO, the only source of phenolic groups (aromatic hydroxyl sites) would be at the sheet periphery. Such sites are very few, however, for the GO sheets of microscale lateral dimension (L ~ 1 μm) used here and in most

other studies. The ratio of basal-to-edge sites scales as $L_{sheet}/L_{C\text{-}C\text{-}bond}$, which is of order 10^3 for microscale sheets. Even if phenolic OH groups were to cover the entire GO edge, at 1:1000 edge-to-basal-site ratio, phenols cannot realistically contribute a significant fraction of the total hydroxyl sites in GO. Most OH in GO must be non-phenolic, and this is consistent with the low H-donor antioxidant activity observed here.

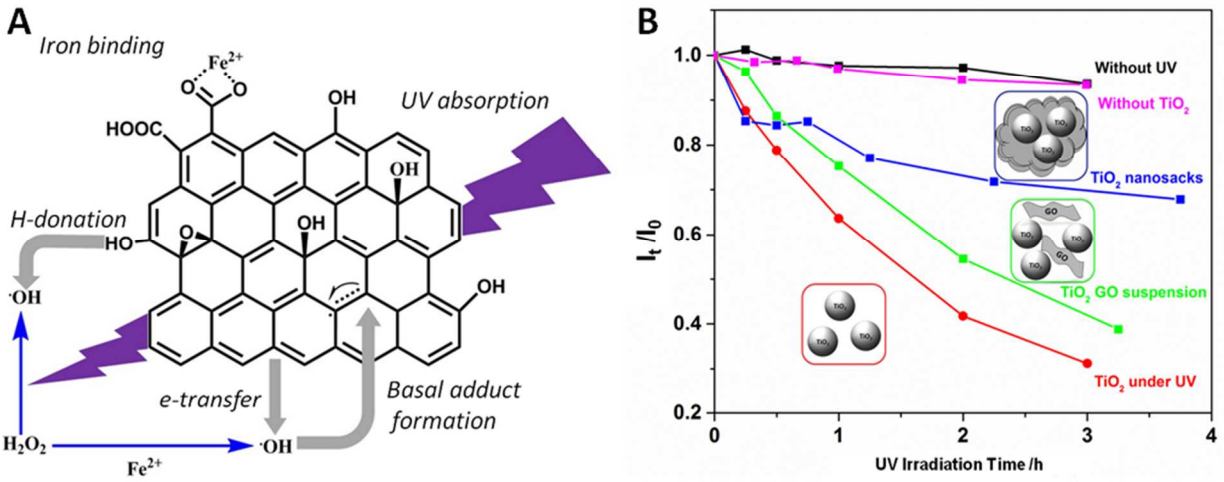

Figure 7. Antioxidant mechanisms and example application. A: Overview of relevant antioxidant mechanisms (UV absorption, iron binding, ·OH adduct formation on sp^2–carbon sites; electron transfer, and hydrogen donation). This study shows that the primary antioxidant activity for graphene-based materials is against ·OH and is associated with pristine sp^2-carbon domains. Hydrogen donation activity is limited by the low population of phenolic OH, which are found on edge but not basal sites. B: Example application of graphene-based oxidation protection. TiO_2-mediated photocatalytic destruction of Rhodamine B dye in the presence and absence of graphene-based materials when exposed to 365 nm long-wavelength UV. Addition of GO (final concentration 20 ppm) in suspension slightly inhibits dye destruction. Encapsulation of TiO_2 in graphene nanosacks (0.1 mg mL^{-1} nanosacks with ~80 wt% TiO_2 and ~20 wt% rGO) significantly inhibits dye oxidation. ROS produced at TiO_2 surfaces are scavenged by internal rGO surfaces prior to release and dye oxidation.

Figure 7A summarizes the behaviors observed in this study. Graphene-based materials are effective scavengers hydroxyl radical, and show some activity toward superoxide. The primary radical scavenging sites are believed to be associated with the pristine sp^2-carbon domains, which act through adduct formation[27] or electron transfer. Graphene-based materials may also act as preventative antioxidants through UV absorption during photochemical ROS formation. Graphene-based materials including GO are weak H-donor antioxidants, which together with the fact that they are large non-diffusible species limits their use to certain applications in oxidation protection. Graphene-based sheet-like materials of microscale lateral dimension can be thought of as stationary, passive scavengers of the more reactive species, such as ·OH, and to be effective in this data, must be present at concentrations on the same order as the target molecules they protect. In some terminologies, materials in this class are referred to oxidation retarders rather than true antioxidants,[60] the latter term being reserved for materials that are effective at much lower concentrations. This pattern of activity suggests two possible antioxidant applications for graphene-based materials:

(1) as fillers or additives in a continuous organic matrix phase, where their ultrahigh surface area provides good site availability and large capacity for ·OH or $\cdot O_2^-$ scavenging. These applications will require high concentrations of the carbon material,[2] in a well-dispersed state, and are thus likely of most interest when the graphene material also provides a second function as a conductive filler or mechanical reinforcement.[61]

(2) as planar films or encapsulation shells where the graphene material serves both as a chemical antioxidant and a physical barrier to oxidant transport to achieve a high degree of oxidation protection. This class of application makes use of the unique 2D geometry of graphene.

As a first demonstration of application type (2) we explored the potential for graphene encapsulation to suppress the release of ROS from TiO_2 nanoparticle surfaces. TiO_2 nanoparticles are widely used in exterior coatings, paints and sunscreens to scatter and absorb potentially damaging ultraviolet radiation (290-400 nm) in sunlight.[62] Ultraviolet photon absorption produces electron-hole pairs in TiO_2 that lead to ROS formation through surface reactions,[63] which in turn causes oxidative damage in the paint, coating, or adjacent skin tissue. Organic and inorganic coatings have been used to suppress ROS formation and protect the product or tissue.[64, 65] The present results suggest that graphene-based materials may be effective in this role both through UV adsorption and radical quenching if a suitable TiO_2-graphene hybrid architecture can be designed.

One possible architecture involves graphene encapsulation, which has been demonstrated through electrostatic wrapping[66, 67] or through continuous aerosol microdroplet drying to form filled graphene nanosacks.[68-70] An important pathway for TiO_2-mediated oxidative damage involves ·OH production according to: $OH^- + hole^+ \rightarrow \cdot OH$[71] followed by ·OH diffusion from the surface to attack adjacent molecular targets. In a TiO_2-filled graphene

nanosack, these surface hole sites would exist only inside the folded sack, and the ·OH produced would have to diffuse through the porous interior and around internal graphene structures to reach surrounding tissue. We hypothesized that the high reactivity of ·OH toward graphenic surfaces would lead to quenching before radical release, and that graphene sack encapsulation would be effective at mitigating TiO_2 nanoparticle-induced oxidative damage.

Figure 7B shows the effect of graphene-based materials on TiO_2-induced photocatalytic dye destruction. TiO_2 nanoparticles alone catalyze the destruction of most of the dye (Rhodamine B) within 3 hrs, and addition of GO in co-suspension has a slight inhibitory effect under these conditions. Much more significant inhibition is seen when all of the TiO_2 particles are encapsulated in folded graphene nanosacks, which are known to be multilayer (3-10) rGO structures whose irregular folding allows rapid diffusional exchange of solutes in aqueous phases,[68] here oxygen and ROS. The overall antioxidant function seen in Figure 7B is believed to be a combination of UV absorption, ROS scavenging in the graphene sack interior, and possible passivation of a portion of the TiO_2 surfaces by close contact with internal conforming graphene structures (see SI) in a manner analogous to the passivation of silica by carbon black following co-grinding to produce intimate contact.[72]

It is interesting that some other studies report the opposite trend - *increases* in TiO_2 photochemical activity following hybridization with graphene.[73, 74] These prior studies fabricate TiO_2 nanostructures bound to planar graphene sheets and attribute the enhancement to electron transfer from TiO_2 to graphene, which reduces electron-hole recombination and improves the photochemical efficiency. This same effect may be present in the data in Figure 7B, but is overwhelmed by the antioxidant function in the nanosack configuration, and the net result is significant inhibition of ROS and oxidative damage. We believe this is a unique behavior of the sack-cargo architecture, which places the oxidizing sites (holes) entirely inside a porous graphenic structure that provides numerous sites for radical scavenging before ROS species can be released to the surrounding medium. This simple demonstration suggests that graphene sack encapsulation may be useful for managing the environmental and health risks associated with some nanoparticle-based technologies.

4. Materials and Methods

4.1. Materials

GO was prepared using a modified Hummers method and purified as described previously.[68] RGO was produced by heating multilayer GO flakes at 250 C for 30 min in nitrogen flow. Few layer graphene (3-5 layers with nominal lateral dimension of 800 nm) was obtained commercially and characterized. Ascorbic acid, titanium (IV) oxide (TiO_2) nanopowders (<25 nm particle size, >99.5 % trace metal basis), iron (II) sulfate haptahydrate ($FeSO_4 \cdot 7H_2O$), reduced GSH, D-mannitol, pC60, xanthine, xanthine oxidase from bovine milk grade IV,2,2'-azobis(2-amidinopropane) hydrochloride (AAPH), thiobarbituric acid (TBA), trichloricacetic acid (TCA), DPPH, 2-deoxy-D-ribose (deoxyribose), sodium dodecyl sulfate (SDS), ABTS, β-Nicotinamide adenine dinucleotide 2'-phosphate reduced tetrasodium salt hydrate (NADH), phenazinemethosulfate (PMS), xanthine, xanthine oxidase from bovine milk, and NBT were purchased from Sigma Chemicals Co (St. Louis, MO). Hydrogen peroxide (H_2O_2), phosphate buffered saline (PBS) (pH 7.4), and EDTA were purchased from Fisher Scientific Inc. (Pittsburgh, PA). 5,5-dimethyl-1-pyrroline-N-oxide (DMPO) were purchased from Dojindo Molecular Technologies, Inc. (Rockville, MD). ThioGlo-1 Fluorescent Thiol Reagent is purchased from EMD Millipore Chemical (Darmstadt, Germany), Nanopure water was used throughout.

4.2. Characterization

The morphologies of all the graphene-based materials were characterized with a LEO 1530 field-emision scanning electron microscope (SEM) and an FEI CM20 TEM. The graphenic structure was characterized with a WITECAlpha 300S Scanning Near-field Optical Microscope with micro Raman system using the 532 nm laser. The functional groups on the graphenic plane and edges were identified using a JASCO FT/IR-4100 Fourier Transform Infrared Spectrometer. N_2 vapor isotherms at 77 K and CO_2 vapor isotherms at 273K were measured using Autosorb-1 instrument from Quantachrome Corporation from which surface areas were calculated by applying Brunauer Emmett Teller (BET) model, and pore size distributions by using carbon slit pore model nonlocal density functional theory (NL-DFT).[75] The size of TiO_2 nanoparticles were found to be around 20~30 nm with TEM and about 57 nm with dynamic light scattering (DLS). The dominant phase was identified to be anatase with X-ray Diffraction (XRD) pattern on a Bruker AXS D8 Advance instrument with Cu KR radiation (λ = 1.5418 Å) (see SI).

4.3. Dye protection assay for •OH scavenging

Phenol red was used as a model target molecule for oxidant attack, and the effects of graphene-based materials on its decoloration rate in the presence of hydroxyl radical used as a measure of antioxidant activity. 10 mL solutions (pH 6.2) containing phenol red (0.1 mM), $FeCl_2$ (0.5□M), H_2O_2 (50 mM) and graphene-based materials (0.10 g L^{-1}) in PBS (50 mM) were continuously stirred on a rotator for 8 hours. 1.5 mL solutions were taken out, centrifuged at 12,000 rpm to remove graphene-based materials and then the absorption spectra of the supernatant were measured with a JASCO V-630 UV/Vis Spectrometer.

4.4. •OH scavenging assay by EPR

EPR spectra were obtained using a Bruker EMXplus spectrometer with procedures similar to our previous research.[76] Spectra were obtained at center field of 3519 G; sweep width 100 G; microwave power 2 mW; sweep time 30 s; number of scans 10; modulation amplitude 1 G; time constant, 81.92 ms. ·OH were generated *in situ* through three methods: Fenton reactions, UV

photolysis and sonochemical cleavage of H_2O_2. In the former method, 180 μL solution containing DMPO (11 mM), H_2O_2 (1.1 mM), graphene-based materials (GO, rGO, FLG, etc) (up to 222 ppm) in PBS (5.5 mM, pH 3) was prepared in a centrifuge tube. Fe(II) (20 μL, 1.0 ppm) aqueous solution freshly prepared from $FeSO_4$ was then added to initiate the reaction. After brief stirring, about 50 μL of solution was then transferred into a capillary tube, which was in turn mounted onto the EPR spectrometer for scanning. The scanning started exactly 20 min after the addition of Fe (II) solution. In the latter method, a solution containing DMPO (1 mM), H_2O_2 (1 mM), GO aqueous solution (up to 20 ppm) in PBS (100 mM, pH 7.4) in a quartz cuvette was exposed to UV light (365 nm at ~10 mW cm^{-2}) for 20 min. 50 μL of the solution was then transferred into a capillary tube, which was in turn mounted onto the EPR spectrometer for scanning.

4.5. Non-enzymatic superoxide radical scavenging assay

The interaction of graphene-based materials with superoxide anion was investigated using the NADH/PMS reaction system to generate superoxide in a method similar to Valentao et al.[44] In a 96-well plate, 200 μL solution containing NADH (200 μM), NBT (50 μM), and test materials (100 ppm) in PBS (20 mM) was prepared and the reaction initiated by addition of PMS (40 μL, 15 μM). The absorption at 560 nm was monitored with a Molecular Device SpectraMax M2 Multimode Microplate Reader for 10 min at room temperature.

4.6. Enzymatic superoxide radical scavenging assay

Here superoxide radicals were generated using the xanthine/xanthine oxidase system using a procedure similar to Valentao et al.[44] In 96-well plates, 200 μL solution containing xanthine (2.0 mM), NBT (50 μM), sample solution (100 ppm), EDTA (0.5 mM) in PBS (20 mM) was prepared and the reaction initiated by addition of xanthine oxidase (5 μL, 20 unit mL^{-1}). Optical absorption at 560 nm was monitored with Molecular Device SpectraMax M2 Multimode Microplate Reader for 10min at room temperature.

4.7. DPPH• and ABTS•$^+$ scavenging assay

DPPH• and ABTS•$^+$ are both relatively stable radicals and are often used to assess antioxidant activity of substances.[48, 52] A procedure similar to that reported by Fukumoto et al [33] was used here in which DPPH• concentration is monitored through its characteristic absorption around 515 nm. 1000 μL of DPPH• (200 μM) solution freshly prepared with 80% methanol and PBS (20 mM, pH 7.4) were mixed with 111 μL aqueous suspensions of the test samples (1.0 g L^{-1}). The mixtures were then left in the dark at room temperature (25 °C) and the optical absorption at 516 nm were measured at regular time intervals up to 680 min.

A modified procedure from Re et al [50] was applied to serve similar purpose with ABTS•$^+$ here. Briefly, ABTS (7 mM) aqueous solution was prepared and activated by potassium persulfate at room temperature for 12-16 hours before use. The activated ABTS•$^+$ radical is stable in the dark for up to 2 days. The free radical solution is diluted with PBS (100 mM, pH 7.4) to get a solution with absorbance of around 0.70 at 734 nm. The aqueous solution of tested materials (100 μL, 2000 ppm) or nanopure water (100 μL) as control is added into the above solution (1.0 mL). The absorbance is recorded every 1 min after the addition of the tested solution.

4.8. GSH competitive oxidation assay

Experiments were performed to test whether the presence of graphene-based materials in suspension could protect GSH from oxidation by hydrogen peroxide. The extent of GSH oxidation was determined by measuring unreacted thiol groups using ThioGlo 1 fluorescent reagent.[13] Briefly, a solution containing GSH (4 mM), H_2O_2 (1 mM), and graphene-based materials (40 ppm) in PBS (100 mM, pH 7.4) were stirred with rotator for 2 h and then filtered through Amicon Ultra-4 Centrifugal Filter Unit with an Ultracel-3 membrane. The filtrates were collected and incubated with ThioGlo-1 (20 μM) in the dark for 30 min after which fluorescence emission was measured at 513 nm (excitation at 379 nm) with the SpectraMax M2 Microplate Reader.

4.9. MDA assay

The effect of graphene-based materials on the $^{\cdot}$OH-mediated oxidation of deoxyribose was studied using an MDA assay modified from Halliwell and Gutteridge.[77] Briefly, freshly prepared deoxyribose (100 mM) solution was mixed with Fenton reagents ($FeCl_2$ and H_2O_2) and FLG or GO suspension to get a solution containing FLG or GO (100 ppm) and deoxyribose (6.7 mM). An equivalent volume of TCA (3% w/v) aqueous solution was added after 20 min incubation at room temperature to stop the Fenton reaction. The solution was then filtered through 0.2 μm membrane to remove the FLG or GO. Part of the filtrate (2 mL) was moved into a test tube and TBA (1 mL, 1%) aqueous dispersion was added. The test tube was kept in a boiling water bath for 15 min to develop the pink chromogen. The tube was then cooled down in another water bath at room temperature for 10 min. The solution was then moved into cuvette and absorbance by the pink chromogen at 532 nm was then recorded with a JASCO V-630 UV/Vis Spectrometer. To rule out adsorptive artifacts, the ability of FLG to physically adsorb deoxyribose was characterized by pre-incubating deoxyribose solutions with FLG for 10 min and then removing the solids with filtration. The filtrate was then incubated with the Fenton reagents and the pink chromogen was developed and measured in the same way. To further test for artifacts involving MDA adsorption, the same Fenton reaction was carried out without FLG for 20 min after which TCA and FLG were added. After a further 10 min incubation, the FLG was filtered after and the filtrates treated as above to develop and measure the pink chromogen.

4.10. Lipid peroxidation

Linoleic acid oxidation is used as a model in this study. The oxidation is initiated by an azo initiator AAPH.[78] Fresh linoleic acid (150 μL) was dispersed in PBS (150 μL, 50 mM, pH 7.4) with

SDS (10 mM) as surfactant. The solution was then diluted 20 times and added tested materials (200 ppm final concentration). Oxidation is initiated by the addition of AAPH (2.4 mM final concentration) into the above solution preheated in 40 °C water bath. The progress of oxidation was monitored by taking a small sample of the solution and measuring the amount of lipid peroxides, which is determined by boiling the sample with TBA (3% w/v) for 15 min and comparing the absorbance at 531 nm.[79] Higher absorbance indicates lipid oxidized to higher extent.

4.11. TiO_2 encapsulation by graphene for ROS supression

Here 0.01 mM Rhodamine B (RhB) was used to monitor the production of ·OH-induced by UV irradiation (365 nm at ~10 mW cm^{-2}) and the relative quenching ability of GO added. Water is transparent to the wavelength used here.[80] The suspension containing GO (20 ppm) and TiO_2 (80 ppm) looks uniform without agglomeration in PBS (pH 7.4).[81] An intrinsic contact between graphene based materials and TiO_2 is achieved. We used a method similar to a previous study by our group to produce TiO_2 graphene nanosacks.[68] Nanosacks (100 ppm, ~80% TiO_2 and ~20% graphene-based materials) were used for comparison. The mixture of dye, TiO_2 (and GO) in buffer was left for 30 min in darkness under continuous stirring with rotator for physisorption before exposure. After exposed to UV light with a distance of ~5 cm between irradiation source and the solution under continuous stirring for various length of time the solid materials were removed through filtration and the absorbance of RhB was recorded.

5. Conclusions

Here we show that graphene oxide exhibits significant antioxidant activity in the form of hydroxyl and superoxide radical scavenging, and can protect a variety of biomolecular target molecules from oxidation. Few-layer graphene is more active than GO despite its lower surface area, indicating that the main scavenging activity is associated with pristine sp2 carbon domains on basal surfaces rather than H-donation from hydroxyl or hydroquinone groups. In experiments involving UV-induced ·OH generation, the protective effect is a combination of UV absorption by graphene and radical scavenging. The combination of radical scavenging, UV absorption, ultrahigh surface area, and elasticity make graphene materials promising for selected antioxidant applications as dispersed phase fillers, or as conformal encapsulating agents that can mitigate ROS production and toxicity from redox-active nanoparticle cargos.

Acknowledgements

This work was supported by the National Science Foundation (Grants CBET-1132446 and INSPIRE Track 1 CBET-1344097) and the Superfund Research Program of the National Institute of Environmental Health Sciences (Grant P42 ES013660). The work on the catalytic activity of graphene-TiO_2 hybrids was supported by the Brown-Yale Center for the Capture and Conversion of CO_2 (NSF Award CHE-1240020). We also appreciate the support on AFM imaging and Raman spectroscopy from Dr. Guanglai Li at Brown University.

Notes and references

[a] *School of Engineering, Brown University, Providence, RI 02912, USA*
[b] *Department of Chemistry, Brown University, Providence, RI 02912, USA*
[c] *Department of Pathology and Laboratory Medicine, Brown University, Providence, RI 02912, USA*

**Corresponding Author*
E-mail: robert_hurt@brown.edu
Tel.: +1 4018632685
Fax: +1 4018639120

† Electronic Supplementary Information (ESI) available: [details of any supplementary information available should be included here]. See DOI: 10.1039/b000000x/

1. M. Antolovich, P. D. Prenzler, E. Patsalides, S. McDonald and K. Robards, *Analyst*, 2002, **127**, 183-198.
2. P. C. P. Watts, P. K. Fearon, W. K. Hsu, N. C. Billingham, H. W. Kroto and D. R. M. Walton, *J Mater Chem*, 2003, **13**, 491-495.
3. H. Y. Yin, L. B. Xu and N. A. Porter, *Chem Rev*, 2011, **111**, 5944-5972.
4. B. Lipinski, *Oxid Med Cell Longev*, 2011, **2011**, 809696-809704.
5. H. Ohshima, Y. Yoshie, S. Auriol and I. Gilibert, *Free Radical Bio Med*, 1998, **25**, 1057-1065.
6. B. M. Silva, P. B. Andrade, P. Valentao, F. Ferreres, R. M. Seabra and M. A. Ferreira, *J Agric Food Chem*, 2004, **52**, 4705-4712.
7. K. Pyrzynska and A. Pekal, *Analytical Methods*, 2013, **5**, 4288-4295.
8. P. G. Pietta, *J Nat Prod*, 2000, **63**, 1035-1042.
9. E. M. Christenson, J. M. Anderson and A. Hiltner, *J Biomed Mater Res A*, 2006, **76A**, 480-490.
10. G. R. Buettner and B. A. Jurkiewicz, *Radiat Res*, 1996, **145**, 532-541.
11. E. S. Almeida, F. M. Portela, R. M. F. Sousa, D. Daniel, M. G. H. Terrones, E. M. Richter and R. A. A. Munoz, *Fuel*, 2011, **90**, 3480-3484.
12. C. K. Sen, S. Khanna, G. Gordillo, D. Bagchi, M. Bagchi and S. Roy, *Ann Ny Acad Sci*, 2002, **957**, 239-249.
13. X. Y. Liu, S. Sen, J. Y. Liu, I. Kulaots, D. Geohegan, A. Kane, A. A. Puretzky, C. M. Rouleau, K. L. More, G. T. R. Palmore and R. H. Hurt, *Small*, 2011, **7**, 2775-2785.
14. L. M. Pasquini, R. C. Sekol, A. D. Taylor, L. D. Pfefferle and J. B. Zimmerman, *Environ Sci Technol*, 2013, **47**, 8775-8783.
15. L. Wang, A. Ambrosi and M. Pumera, *Angew Chem Int Edit*, 2013, **52**, 13818-13821.
16. A. Ambrosi and M. Pumera, *Nanoscale*, 2014, **6**, 472-476.
17. L. Guo, D. G. Morris, X. Liu, C. Vaslet, R. H. Hurt and A. B. Kane, *Chemistry of Materials*, 2007, **19**, 3472-3478.
18. W. Z. Teo, E. L. Chng, Z. Sofer and M. Pumera, *Nanoscale*, 2014, **6**, 1173-1180.
19. E. L. Chng, Z. Sofer and M. Pumera, *Chemistry*, 2014, **20**, 6366-6373.
20. E. L. K. Chng and M. Pumera, *Chemistry – A European Journal*, 2013, **19**, 8227-8235.

21. R. M. Lucente-Schultz, V. C. Moore, A. D. Leonard, B. K. Price, D. V. Kosynkin, M. Lu, R. Partha, J. L. Conyers and J. M. Tour, *J Am Chem Soc*, 2009, **131**, 3934-3941.
22. L. Y. Chiang, F. J. Lu and J. T. Lin, *J Chem Soc Chem Comm*, 1995, 1283-1284.
23. K. Okuda, T. Hirota, M. Hirobe, T. Nagano, M. Mochizuki and T. Mashino, *Fullerene Sci Techn*, 2000, **8**, 127-142.
24. I. Fenoglio, M. Tomatis, D. Lison, J. Muller, A. Fonseca, J. B. Nagy and B. Fubini, *Free Radical Bio Med*, 2006, **40**, 1227-1233.
25. A. Galano, *J Phys Chem C*, 2008, **112**, 8922-8927.
26. R. Martin, C. Menchon, N. Apostolova, V. M. Victor, M. Alvaro, J. R. Herance and H. Garcia, *Acs Nano*, 2010, **4**, 6957-6965.
27. B. R. Bitner, D. C. Marcano, J. M. Berlin, R. H. Fabian, L. Cherian, J. C. Culver, M. E. Dickinson, C. S. Robertson, R. G. Pautler, T. A. Kent and J. M. Tour, *Acs Nano*, 2012, **6**, 8007-8014.
28. G. W. Burton and K. U. Ingold, *Science*, 1984, **224**, 569-573.
29. A. Martinez and A. Galano, *J Phys Chem C*, 2010, **114**, 8184-8191.
30. Y. Morita, S. Suzuki, K. Sato and T. Takui, *Nat Chem*, 2011, **3**, 197-204.
31. J. S. Wright, E. R. Johnson and G. A. DiLabio, *J Am Chem Soc*, 2001, **123**, 1173-1183.
32. W. Bors, W. Heller, C. Michel and M. Saran, *Method Enzymol*, 1990, **186**, 343-355.
33. L. R. Fukumoto and G. Mazza, *J Agric Food Chem*, 2000, **48**, 3597-3604.
34. E. Graf, J. R. Mahoney, R. G. Bryant and J. W. Eaton, *J Biol Chem*, 1984, **259**, 3620-3624.
35. D. Lozano-Castello, D. Cazorla-Amoros and A. Linares-Solano, *Carbon*, 2004, **42**, 1233-1242.
36. Y. Qiu, F. Guo, R. Hurt and I. Külaots, *Carbon*, 2014, **72**, 215–223.
37. F. Guo, M. Creighton, Y. T. Chen, R. Hurt and I. Kulaots, *Carbon*, 2014, **66**, 476-484.
38. Y. Ku, Y. H. Tu and C. M. Ma, *Water Res*, 2005, **39**, 1093-1098.
39. A. De Visscher and H. Van Langenhove, *Ultrason Sonochem*, 1998, **5**, 87-92.
40. M. A. Creighton, J. R. Rangel-Mendez, J. Huang, A. B. Kane and R. H. Hurt, *Small*, 2013, **9**, 1921-1927.
41. M. J. Burkitt and B. C. Gilbert, *Free Radical Res Com*, 1990, **10**, 265-280.
42. A. J. Nappi and E. Vass, *Biochimica et biophysica acta*, 1997, **1336**, 295-302.
43. J. Limon-Pacheco and M. E. Gonsebatt, *Mutation research*, 2009, **674**, 137-147.
44. P. Valentao, E. Fernandes, F. Carvalho, P. B. Andrade, R. M. Seabra and M. L. Bastos, *J Agric Food Chem*, 2001, **49**, 3476-3479.
45. M. Nishikimi, *Biochem Bioph Res Co*, 1975, **63**, 463-468.
46. B. Halliwell and C. H. Foyer, *The Biochemical journal*, 1976, **155**, 697-700.
47. E. Niki, *Am J Clin Nutr*, 1991, **54**, S1119-S1124.
48. J. J. Yin, F. Lao, P. P. Fu, W. G. Wamer, Y. Zhao, P. C. Wang, Y. Qiu, B. Sun, G. Xing, J. Dong, X. J. Liang and C. Chen, *Biomaterials*, 2009, **30**, 611-621.
49. C. N. Murthy and K. E. Geckeler, *Chemical Communications*, 2001, 1194-1195.
50. R. Re, N. Pellegrini, A. Proteggente, A. Pannala, M. Yang and C. Rice-Evans, *Free Radical Bio Med*, 1999, **26**, 1231-1237.
51. X. R. Xia, N. A. Monteiro-Riviere and J. E. Riviere, *Toxicol Lett*, 2010, **197**, 128-134.
52. M. S. Blois, *Nature*, 1958, **181**, 1199-1200.
53. M. Valko, D. Leibfritz, J. Moncol, M. T. Cronin, M. Mazur and J. Telser, *The international journal of biochemistry & cell biology*, 2007, **39**, 44-84.
54. N. Ballatori, S. M. Krance, S. Notenboom, S. Shi, K. Tieu and C. L. Hammond, *Biological chemistry*, 2009, **390**, 191-214.
55. Q. Y. Zhu, X. M. Zhang and A. J. Fry, *Polym Degrad Stabil*, 1997, **57**, 43-50.
56. S. Kim, S. Zhou, Y. K. Hu, M. Acik, Y. J. Chabal, C. Berger, W. de Heer, A. Bongiorno and E. Riedo, *Nat Mater*, 2012, **11**, 544-549.
57. C.-T. Ho, in *Phenolic Compounds in Food and Their Effects on Health II*, American Chemical Society, 1992, vol. 507, ch. 1, pp. 2-7.
58. S. A. Everett, M. F. Dennis, K. B. Patel, S. Maddix, S. C. Kundu and R. L. Willson, *J Biol Chem*, 1996, **271**, 3988-3994.
59. Y. Qin and R. A. Wheeler, *J Phys Chem-Us*, 1996, **100**, 10554-10563.
60. E. M. Becker, L. R. Nissen and L. H. Skibsted, *Eur Food Res Technol*, 2004, **219**, 561-571.
61. T. Ramanathan, A. A. Abdala, S. Stankovich, D. A. Dikin, M. Herrera-Alonso, R. D. Piner, D. H. Adamson, H. C. Schniepp, X. Chen, R. S. Ruoff, S. T. Nguyen, I. A. Aksay, R. K. Prud'homme and L. C. Brinson, *Nat Nanotechnol*, 2008, **3**, 327-331.
62. Z. A. Lewicka, A. F. Benedetto, D. N. Benoit, W. W. Yu, J. D. Fortner and V. L. Colvin, *J Nanopart Res*, 2011, **13**, 3607-3617.
63. R. Dunford, A. Salinaro, L. Cai, N. Serpone, S. Horikoshi, H. Hidaka and J. Knowland, *Febs Lett*, 1997, **418**, 87-90.
64. J. Xiao, W. Chen, F. Wang and J. Du, *Macromolecules*, 2013, **46**, 375-383.
65. G. Wakefield, M. Green, S. Lipscomb and B. Flutter, *Mater Sci Tech-Lond*, 2004, **20**, 985-988.
66. R. Kempaiah, S. Salgado, W. L. Chung and V. Maheshwari, *Chemical Communications*, 2011, **47**, 11480-11482.
67. X. Wen, C. W. Garland, T. Hwa, M. Kardar, E. Kokufuta, Y. Li, M. Orkisz and T. Tanaka, *Nature*, 1992, **355**, 426-428.
68. Y. Chen, F. Guo, Y. Qiu, H. Hu, I. Kulaots, E. Walsh and R. H. Hurt, *Acs Nano*, 2013.
69. J. Y. Luo, H. D. Jang, T. Sun, L. Xiao, Z. He, A. P. Katsoulidis, M. G. Kanatzidis, J. M. Gibson and J. X. Huang, *Acs Nano*, 2011, **5**, 8943-8949.
70. X. F. Ma, M. R. Zachariah and C. D. Zangmeister, *Nano Letters*, 2012, **12**, 486-489.
71. A. L. Linsebigler, G. Q. Lu and J. T. Yates, *Chem Rev*, 1995, **95**, 735-758.
72. M. Ghiazza, M. Tomatis, S. Doublier, F. Grendene, E. Gazzano, D. Ghigo and B. Fubini, *Chemical research in toxicology*, 2013, **26**, 46-54.
73. R. Sellappan, J. Sun, A. Galeckas, N. Lindvall, A. Yurgens, A. Y. Kuznetsov and D. Chakarov, *Physical chemistry chemical physics : PCCP*, 2013, **15**, 15528-15537.
74. Y. Zhang, Z. R. Tang, X. Fu and Y. J. Xu, *Acs Nano*, 2010, **4**, 7303-7314.

75. C. Lastoskie, K. E. Gubbins and N. Quirke, *Langmuir*, 1993, **9**, 2693-2702.
76. Z. Wang, A. von dem Bussche, P. K. Kabadi, A. B. Kane and R. H. Hurt, *Acs Nano*, 2013, **7**, 8715-8727.
77. B. Halliwell and J. M. C. Gutteridge, *Febs Lett*, 1981, **128**, 347-352.
78. M. N. Peyrat-Maillard, M. E. Cuvelier and C. Berset, *J Am Oil Chem Soc*, 2003, **80**, 1007-1012.
79. H. Ohkawa, N. Ohishi and K. Yagi, *J Lipid Res*, 1978, **19**, 1053-1057.
80. R. A. J. Litjens, T. I. Quickenden and C. G. Freeman, *Appl Optics*, 1999, **38**, 1216-1223.
81. J. M. Berg, A. Romoser, N. Banerjee, R. Zebda and C. M. Sayes, *Nanotoxicology*, 2009, **3**, 276-283.